Int J Biometeorol
DOI 10.1007/s00484-016-1277-x

ORIGINAL PAPER

Nonlinear variations of forest leaf area index over China during 1982–2010 based on EEMD method

Yunhe Yin[1] · Danyang Ma[1,2] · Shaohong Wu[1] · Erfu Dai[1] · Zaichun Zhu[3] · Ranga B. Myneni[4]

Received: 8 December 2015 / Revised: 28 August 2016 / Accepted: 15 November 2016

Abstract Variations in leaf area index (LAI) are critical to research on forest ecosystem structure and function, especially carbon and water cycle, and their responses to climate change. Using the ensemble empirical mode decomposition (EEMD) method and global inventory modeling and mapping studies (GIMMS) LAI3g dataset from 1982 to 2010, we analyzed the nonlinear feature and spatial difference of forest LAI variability over China for the past 29 years in this paper. Results indicated that the national-averaged forest LAI was characterized by quasi-3- and quasi-7-year oscillations, which generally exhibited a rising trend with an increasing rate. When compared with 1982, forest LAI change by 2010 was more evident than that by 1990 and 2000. The largest increment of forest LAI occurred in Central and South China, while along the southeastern coastal areas LAI increased at the fastest pace. During the study period, forest LAI experienced from decrease to increase or vice versa across much of China and varied monotonically for only a few areas. Focusing on regional-averaged trend processes, almost all eco-geographical regions showed continuously increasing trends in forest LAI with different magnitudes and speeds, other than tropical humid region and temperate humid/subhumid region, where LAI decreased initially and increased afterwards.

Keywords Leaf area index · Forest · Variations · EEMD method

✉ Yunhe Yin
yinyh@igsnrr.ac.cn

1 Key Laboratory of Land Surface Pattern and Simulation, Institute of Geographic Sciences and Natural Resources Research, Chinese Academy of Sciences, 11A, Datun Road, Chaoyang District, Beijing 100101, China

2 University of Chinese Academy of Sciences, 19A Yuquan Road, Shijingshan District, Beijing 100049, China

3 Sino-French Institute for Earth System Science, College of Urban and Environmental Sciences, Peking University, No.5 Yiheyuan Road, Beijing 100871, China

4 Department of Earth and Environment, Boston University, 675 Commonwealth Avenue, Boston, MA 02215, USA

Introduction

As an important component of terrestrial ecosystem, forest plays a key role in coping with climate change, as well as regulating global carbon and water cycle. In the context of changing climate, forest distribution, phenology, productivity, carbon sequestration, and eco-hydrological function would vary accordingly (IPCC 2007). Therefore, clarifying the variability of forest structure and function and assessing the response and adaptation of forest to climate change are crucial issues in global change research. However, owing to the complexity of forest ecosystem, uncertainty of climate change, and limitations of people's cognition, there still exist large disagreements and uncertainties in the above studies (Bonan 2008; Millar et al. 2007). Consequently, we need to precisely describe the growth dynamics and biophysical processes of forest vegetation and analyze its secular variations and influencing factors.

As an important parameter characterizing vegetation canopy structure, leaf area index (LAI) controls many biological and physical processes of vegetation, such as photosynthesis, respiration, transpiration, carbon and nutrient cycle, and rainfall interception (Chen and Cihlar 1996). It affects the exchange of substance, energy, and momentum between land surface and atmosphere (Monteith and Unsworth 1990) and serves as required input or key variable in most ecological models and global models of climate, hydrology, and biogeochemistry (Sellers et al. 1997). Since ground-based methods

Published online: 25 November 2016

for measuring LAI are only proper to obtain LAI on a small scale, large-scale estimation of LAI mainly depend on the development of remote sensing techniques. Approaches for deriving LAI from satellite information can be broadly categorized as empirical methods, physical methods, and machine learning algorithms (Zhu et al. 2013).

Much research on LAI variations has been carried out in recent years. For LAI can be measured at leaf, plant, stand, or community levels, it is able to reflect the spatial heterogeneity of leaf distribution within the canopy and the geographical pattern of regional even global vegetation. It is beneficial to explore spatial variations in LAI for simulating forest growth and projecting forest production. Remote sensing-based LAI data is applied to plenty of climate-vegetation models for validation and evaluation (Buermann et al. 2001; Murray-Tortarolo et al. 2013). For LAI has distinct seasonal and interannual variability, it is equally vital to monitor temporal variations in LAI for understanding terrestrial ecosystem fluxes and their feedbacks to global change. Climatic factors including radiation, temperature, and precipitation would alter leaf carbon uptake in time and intensity by affecting LAI circulation and extremes, thus impacting vegetation photosynthesis capacity and productivity (Barr et al. 2004; Campioli et al. 2009; Muraoka et al. 2010).

Long-term and continuous remote sensing observation with high temporal resolution provides important data source to vegetation dynamic research. Various statistical means and frequency-spectral techniques (Bradley et al. 2007; Lasaponara 2006; Martínez and Gilabert 2009) are gradually applied to the processing and analyzing of vegetation remote sensing. Under the background of climate change, research shows that global-averaged LAI has exhibited a rising trend for decades, especially significant in the middle and high latitudes of North Hemisphere, which was mainly attributed to a lengthening of growing season caused by global warming (Liu et al. 2010; Mao et al. 2013; Piao et al. 2006). China's vegetation LAI was supposed to follow a similar trend (Piao et al. 2015; Xiao and Moody 2010). Nevertheless, time series analysis is traditionally under the premise of linear and stationary assumption, following which long-period oscillations may be confused with trend variations. Actually, vegetation time series are nonlinear and nonstationary processes which contain a combination of seasonal, gradual, and abrupt changes (Henebry and Beurs 2005; Verbesselt et al. 2010). It is necessary to choose a suitable method that allows discussing the periodicity and tendency of LAI via temporal-spatial data, in order to grasp multi-scale variations of vegetation and its relationship with climate change. Nowadays, some nonlinear fitting methods have provided a new way to analyze time series. Methods accounting for nonlinearity are able to separate series into components of different time scales and meanwhile preserve the time domain flexibility of signals (Hawinkel et al. 2015). They are more sensitive than simple linear analysis to trend changes within short duration or even reversing changes in long-term time series (Jong et al. 2012), thus potentially deepening understanding of vegetation responses to climatic and human factors. For examples, Breaks For Addictive Seasonal and Trend (BFAST) analysis (Verbesselt et al. 2010) and Detecting Breakpoints and Estimating Segments in Trend (DBEST) analysis (Jamali et al. 2015) focus on rapid and stepwise changes in vegetation effected by disturbances like wildfire and recovery; polynomial fitting-based scheme (Jamali et al. 2014) could automatically divide vegetation changes into cubic, quadratic, linear, and concealed trends; Ensemble Empirical Mode Decomposition (EEMD) method (Wu and Huang 2009) is able to extract periodic signals as well as long-term trend. In addition, most studies aimed at LAI variations on the countrywide scale of China focused on the time-space distribution of LAI in different periods or different vegetation types and its correlation with climatic factors (Huang and Ji 2010; Liu et al. 2012a; Ren et al. 2014). Considering China's vast territory and clear zonality, it will be more appropriate to elaborate the regional differences of vegetation change from the perspective of eco-geographical regionalization.

EEMD (Wu and Huang 2009) is an adaptive and noise-assisted time series analysis method and well suited to deal with nonlinear and nonstationary processes. It can extract fluctuant and trend components with multiple characteristic scales from complicated signals. Compared with empirical orthogonal function and wavelet analysis methods, EEMD does not need any priori hypothesis and bases data decomposition on localized features, whose results have higher time-frequency resolution and clearer physical meaning. By applying EEMD to multi-dimensional data, the spatial structural evolution of periodic oscillations on different time scales is obtained and trend varying with time and space is separated. Currently, EEMD has been successfully and widely used in the field of climate change, but the majority of study objects are meteorological and hydrological elements (Chang et al. 2010; Franzke 2012; Wu et al. 2011). It is still rare to use EEMD and its predecessor the empirical mode decomposition (EMD) to directly analyze remote-sensed vegetation data. That is probably because of the need for long-term and continuous data, whereas most remote sensing data on regional scale began from the 1980s. There is a lack of systematic studies on the application of EEMD to large spatiotemporal datasets, and the significance tests for EEMD components remain controversial (Hawinkel et al. 2015). After decomposing the homogenized daily temperature dataset by means of EEMD and extracting its interannual, interdecadal components and secular trend, an earlier start of spring and lengthening of growing season was found at many locations around the world over the last 100 years (Qian et al. 2011; Xia et al. 2013). Moreover, EEMD was used to reconstruct tree-ring climate series for the past millennia, which was more consistent with existing observations, suggesting EEMD could extract low-frequency signals from proxy data more effectively than conventional methods like ordinary least squares and variances matching method (Shi et al. 2014; Shi et al. 2012). When it comes to vegetation remote sensing, EMD denoising method was implemented to smooth NDVI time series and identify the vegetation degeneration of Northeast India and surrounding regions (Verma and Dutta 2013). However, most of these studies were limited to site data and may have neglected the time-varying nature of trend.

The overall objective of this study is to investigate the nonlinear variations of forest LAI over China during 1982–2010, by applying the EEMD method to the Global Inventory Modeling and Mapping Studies (GIMMS) LAI3g dataset. More specifically, the national-averaged forest LAI variations were analyzed on multiple timescales; the temporal-spatial variability of forest LAI across the country was analyzed based on pixel-level data decomposition; the regional differences of forest LAI changes were illuminated among the eco-geographical regions in China. All the work was done in order to provide a scientific reference for accurately assessing forest carbon and water cycle, deeply studying the responses of forest ecosystem to climate change, and making relative adaptation policies.

Study area

Figure 1 presents the basic distribution of forest in China. Evergreen needle-leaved forest occupies a small area, mainly found in the Tianshan Mountains and the southeast of Tibetan Plateau, where *Picea* and *Abies* are the principle trees. Deciduous needle-leaved forest is concentrated in the north of Daxing'an Mountains, where *Larix gmelinii* is the representative species. Deciduous broad-leaved forest is mainly located in Northeast China and sporadically distributed in Loess Plateau. The dominant trees are represented by *Quercus* of the family *Fagaceae*. Evergreen broad-leaved forest has a relatively big area and continuous distribution, including South China and the southern parts of the East Himalayas. The main trees include *Fagaceae*, *Lauraceae*, and *Theaceae* in the south subtropical zone, and *Dipterocarpaceae*, *Meliaceae*, *Sterculiaceae*, etc. in the tropical rainforests. Mixed forest has the widest distribution, from Northeast China to the east of temperate and subtropical zones. The dominant trees of forest types are referenced from Wu (1980).

Materials and methods

The GIMMS LAI3g product (Zhu et al. 2013) was derived from GIMMS NDVI3g dataset utilizing an artificial neural network model. It adopted geographic coordinate system with a 1/12° spatial resolution and 15-day temporal frequency, covering the time span of January 1982 to December 2010. The valid range of LAI values was defined as 0 to 7. A comprehensive assessment was conducted on LAI3g data, showing a satisfied consistency with 45 sets of field measurements from 29 sites worldwide. Through comparison with the Carbon Cycle and Change in Land Observational Products from an Ensemble of Satellites (CYCLOPES) LAI product on global and site scale, LAI3g was perceived to be much closer to ground truth values, especially in forests (Fang et al. 2012; Zhu et al. 2013).

Land cover data came from the Collection 5 Moderate Resolution Imaging Spectroradiometer (MODIS) land cover-type product (MCD12C1) at a spatial resolution of 0.05° in geographic latitude-longitude projection. It was integrated from both Terra and Aqua satellite observation annually, using a supervised classification algorithm. Cross-validation analysis indicated an overall classification accuracy of 75% for this product (Friedl et al. 2010). According to the International Geosphere Biosphere Programme (IGBP) class, five land cover types related to forest were used in this study (Fig. 1).

Considering that MCD12C1 of 2007 was one of the input data-generating LAI3g, we selected it as a standard for extracting forest pixels, re-sampled it to the same spatial resolution as LAI3g (1/12 × 1/12°), and clipped it with vector boundary of China. Hence, the spatial distribution information of forest cover in China under the IGBP classification system was achieved. Annual averages of 29-year LAI time series were then computed for all forest pixels. Based on eco-geographical regions in China (Zheng 2008), ranging from tropical to cold temperate and from humid to arid, forest LAI in each of the ten regions and the whole country were calculated by pixel area-weighted averaging.

The core idea of EEMD method is to add white noise to the original series $x(t)$ and decompose the mixed data in terms of several amplitude-frequency-modulated oscillatory components C_j (j = 1, 2, …, n) (Eq. 1). By repeating the above steps, the ensemble means will be acquired as the final intrinsic mode functions (IMFs). After enough trials, the added white noise could cancel out, realizing adaptive decomposing within the dyadic filter windows. The number and property of IMFs depend on the data length and local characteristics. EEMD has not only taken the advantage of EMD in the respect of signal processing and time-frequency analysis but also resolved the mode mixing problem thereby ensuring the physical uniqueness of IMFs. The residual component R_n is monotonic or contains at most one extreme, which is believed to have removed inherent fluctuations and reserved secular trend representing the true information of signal. The trend varies with time yet does not depend upon any given shape. It performs better than traditional linear fitting

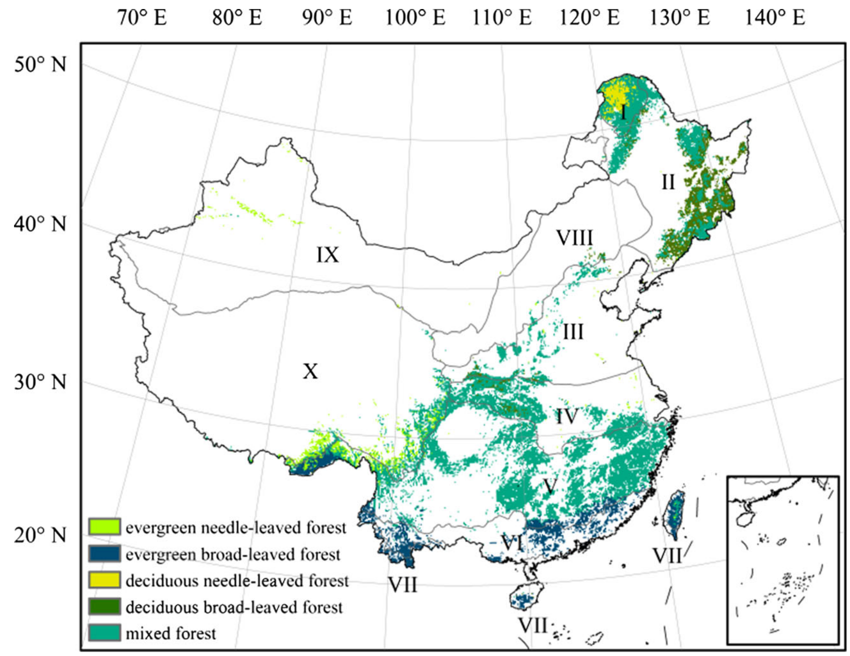

Fig. 1 Forest distribution and eco-geographical regions in China. *I*, Cold temperate humid region; *II*, temperate humid/subhumid region; *III*, warm temperate humid/subhumid region; *IV*, north subtropical humid region; *V*, subtropical humid region; *VI*, south subtropical humid region; *VII*, tropical humid region; *VIII*, north semi-arid region; *IX*, northwest arid region; *X*, Tibetan Plateau region

method in reflecting the potential, nonlinear, and nonstationary characteristics of time series.

In this study, white noise at an amplitude value of 0.2 was added to LAI series with 100 times of trial when using EEMD method at each pixel. The standard deviation of error between the reconstructed and original data series was 0.02. According to the method, the total number of IMFs of a data set is close to $\log_2 N$ with N the number of total data points (Wu and Huang 2009); hence, three IMFs were extracted from our 29-year time series, which is the same for each pixel over the whole area. Each of the resulting IMFs is considered a function having symmetric envelopes around zero defined by the local extrema. Based on this property, the mean period of the IMF could be determined by counting the number of peaks (local maxima) of the function. More details could be found in Wu and Huang (2004). To examine the impacts of all IMFs and residual trend on the original series, we figured out variance contributions and correlation coefficients and also implemented Monte Carlo tests by MATLAB software. The Monte Carlo method uses 1000 samples of randomly generated white noise series with the same data length of LAI time series. Each sample is decomposed into components by EEMD, thus the empirical probability density function (PDF) of residual trend at any temporal location will be obtained. Through comparing the targeted trend value with the two-standard-deviation level of the noise trend PDF, whether it is statistically significant could be judged. Referencing Ji et al. (2014), we represented accumulated LAI changing with the increment of EEMD trend values at a specified time from the starting time of 1982 (Eq. 2). The temporal derivatives of EEMD trend series determined their corresponding LAI changing rates at instantaneous moments (Eq. 3).

$$x(t) = \sum_{j=1}^{n} C_j(t) + R_n(t) \tag{1}$$

$$\mathrm{Trend_{EEMD}}(t) = R_n(t) - R_n(1982) \tag{2}$$

$$\mathrm{Rate_{EEMD}}(t) = \mathrm{d}R_n{}^{(t)} \Big/ \mathrm{d}t \tag{3}$$

Equation 1 shows that in the EEMD approach, a time series at a pixel point $x(t)$ is decomposed in terms of IMFs (C_j) and a residue (R_n). C_j are oscillatory functions with varied amplitude and frequency, while R_n is a monotonic function or a function containing only a single extremum from which no more IMFs can be extracted. In Eq. 2, $\mathrm{Trend_{EEMD}}(t)$ is actually the net increase between the start and end of R_n. When selecting different ending points, different increments relative to the same starting point will be obtained. Equation 3 defines the temporal derivatives of R_n, i.e., $\mathrm{Rate_{EEMD}}(t)$, as the changing rates of EEMD trend.

Results

National-averaged forest LAI variations

National-averaged forest LAI during 1982–2010 was decomposed into three IMFs and a residual (Fig. 2). IMFs reflected the fluctuations of LAI from high frequency to low frequency, respectively, all of which varied with time unevenly. The first two IMFs represented quasi-3- and quasi-7-year

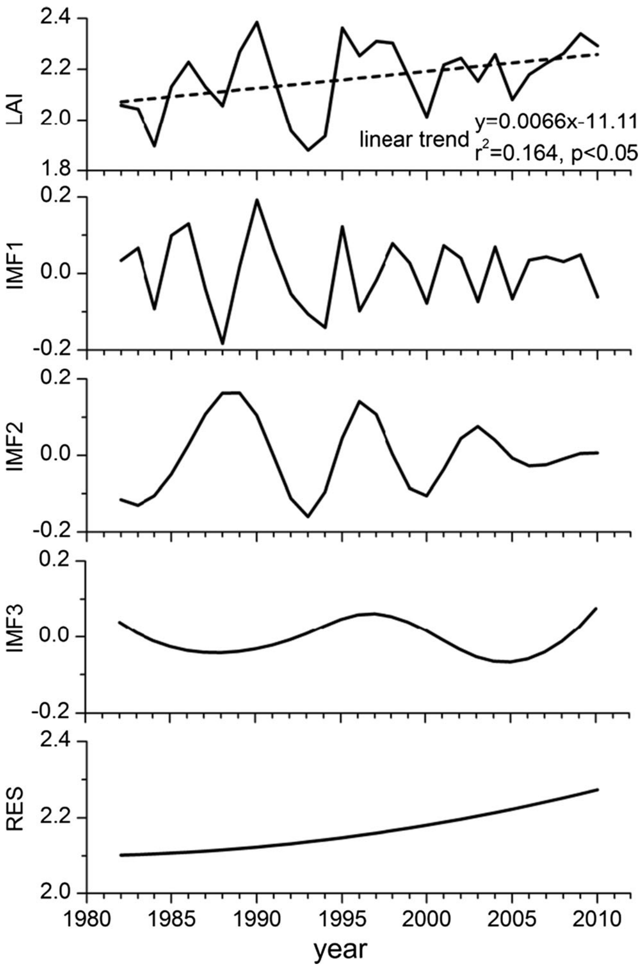

Fig. 2 EEMD components of national-averaged forest LAI

interannual scale oscillations of LAI time series. From Table 1, the first two IMFs had greater variance contributions and were significantly correlated to original series, illustrating that forest LAI variations were chiefly dependent on interannual oscillations with relatively high frequency. The residual component was the overall adaptive trend of LAI for the study period. With fluctuations excluded, LAI changed weakly in the early stage, and then increased gradually and continually before reaching the maximum at final. In consequence, linear fitting method merely simulated a constant rate, and EEMD showed a more detailed changing process of LAI with an increasing rate over time, which could better reveal the non-linear variations of vegetation status.

Temporal-spatial variations of forest LAI in China

EEMD was performed on pixel scale to decompose LAI time series and produce the value increment of trend. The spatial evolution of accumulated change in LAI from 1982 to 1990, 2000, and 2010, respectively, is shown on Fig. 3. Table 2 gives the percentages of pixels with significant LAI change corresponding to every period. It was clear that by 1990, the number of significant pixels, dominantly with increased LAI, was nearly the same as insignificant ones. Forest LAI increase to the south of Qinling Mountain-Huaihe River was generally larger than that to the north. Significant decrease mainly occurred in the southeastern coastal areas and some individual regions of southwest mountains. By 2000, there was a marked improvement on the percentage of significant areas where forest LAI had obvious rise and expanded range. Pixels with significant decrease were substantially located in the edge of forest areas. By 2010, significantly increased forest LAI, ranging from north to south, had occupied two thirds of national forest cover. The increment of LAI trend reached above 0.45 in most parts of Central and South China. In contrast, pixels with significant LAI decrease obviously reduced, whose percentage was even lower than that by 1990. Although the forest LAI increment of linear trend was roughly similar with that of EEMD trend in magnitude and spatial pattern, the linear fitting method could not offer the above trend evolution.

Figure 4 shows the instantaneous rate distribution of forest LAI trend in China respectively in 1990, 2000, and 2010. Except for small areas in East China where LAI slightly declined, most south regions had increasing rates with varying extent in 1990, while Northeast China exhibited relatively low rates of LAI changing. In 2000, areas with negative rates shrank obviously and some places even turned into regions with rapid LAI increase. However, forest LAI in Xiaoxing'an and Changbai Mountains declined sharply. In 2010, areas with positive rates further expanded with many values exceeding 0.03. Meanwhile, the falling down of LAI rates seemed more serious, especially in Qinling Mountains and the southeast of Tibetan Plateau where LAI dropped faster than 0.01. The spatial pattern of LAI

Table 1 Mean periods and variance contributions of EEMD components and their correlation coefficients with the original series of national-averaged forest LAI

	Mean period (year)	Variance contribution (%)	Correlation coefficient
IMF1	2.9	37.92	0.634**
IMF2	7.3	40	0.636**
IMF3	14.5	8.42	0.113
RES	–	13.66	0.394*

*0.05 confidence level; **0.01 confidence level—statistical significance

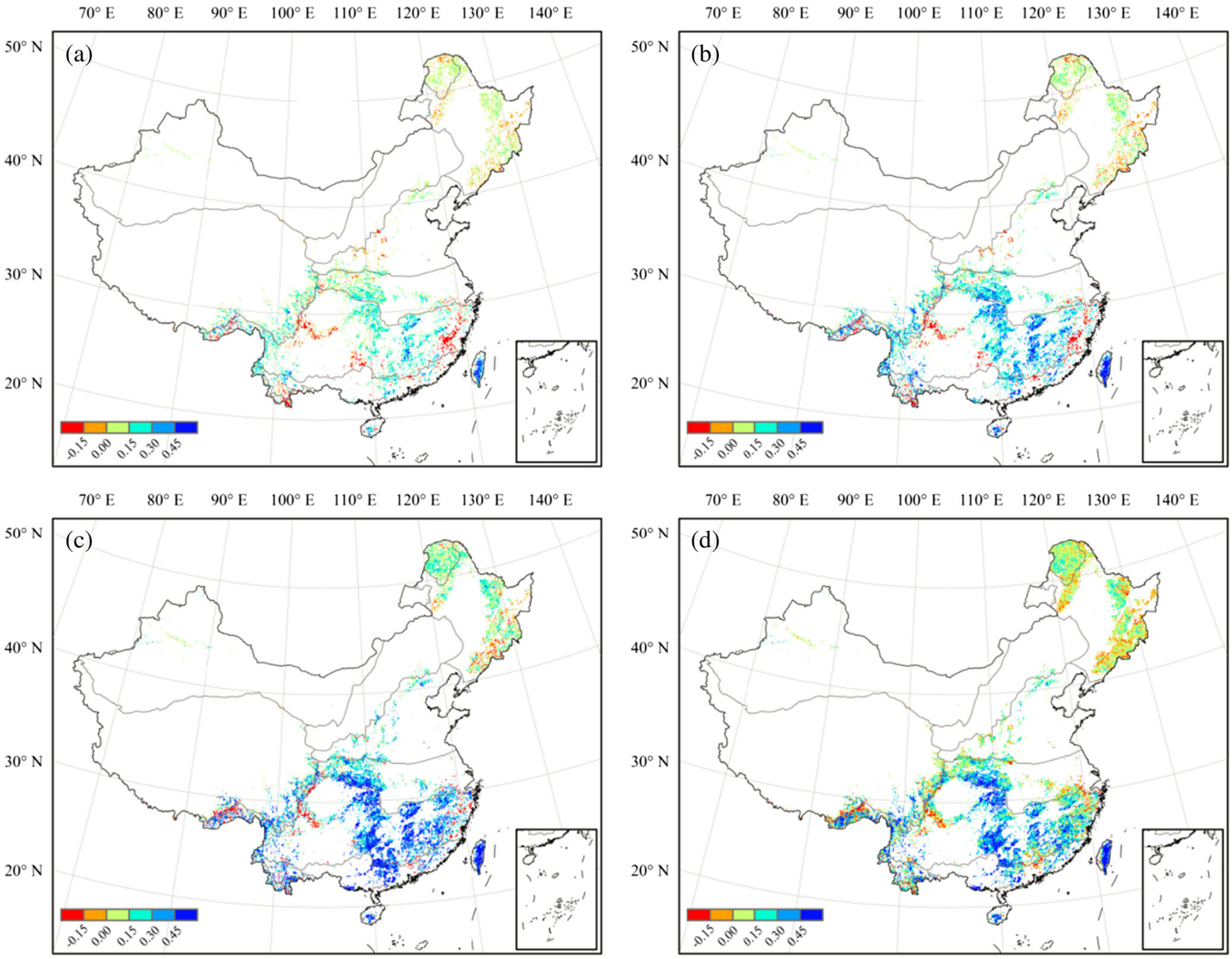

Fig. 3 Forest LAI increment based on EEMD trend ending in 1990 (**a**), 2000 (**b**), and 2010 (**c**) and based on linear trend during 1982–2010 (**d**). Note that the pixel values in (**a**), (**b**), and (**c**) were calculated using Eq. 2, with only significant values preserved

changing rates simulated by linear fitting method was broadly consistent with that by EEMD method but at weaker pace entirely and failed to reflect that the time-varying feature of LAI trend.

Since the EEMD residual component is monotonic or contains at most one extreme, the trend shape could be monotonically increasing or decreasing curve. However, when the trend contains one and only one extreme within the data span, it would show a changing feature from increasing to decreasing or vice versa. Therefore, in this study, we classified forest LAI trend shapes based on EEMD residuals into four types over the whole area (Fig. 5). Results showed that the percentages of pixels with trend changing from increasing to decreasing and the opposite were about 27% and 35%. Pixels with monotonically increasing and decreasing trend occupied approximately 35% and 3%. Apparently, the long-term trend of forest LAI in most areas had transitions. Areas where LAI fell first and rose then were centered in Daxing'an Mountains and the southeastern coastal areas. Areas where LAI rose first and fell then scattered from Northeast China to Southwest China. In Central and South China as well as South Yangzi River, forest LAI increased monotonically. Results from linear fitting method could only reflect monotonic variations likely masking the changing stages. For instance, LAI in the east of Daxing'an Mountains displayed a linearly decreasing

Table 2 Percentages of pixels with significant increment of forest LAI based on EEMD trend

	1982–1990	1982–2000	1982–2010
Significant increase	40.5	52.44	65.08
Significant decrease	8.77	9.08	8.09
Insignificant change	50.73	38.48	26.83

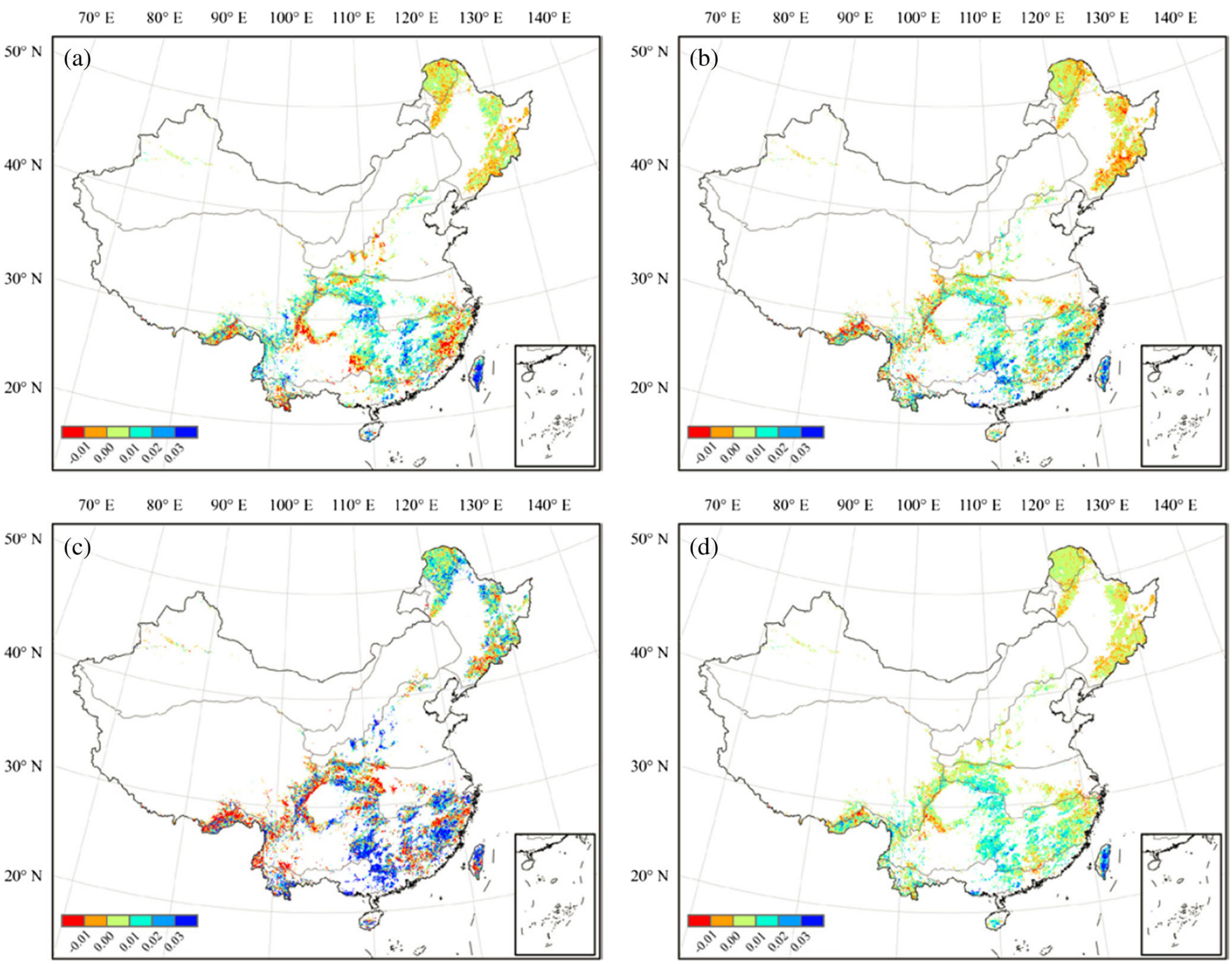

Fig. 4 Forest LAI changing rate based on EEMD trend in 1990 (**a**), 2000 (**b**), and 2010 (**c**) and based on linear trend during 1982–2010 (**d**). Note that the pixel values in (**a**), (**b**), and (**c**) were calculated using Eq. 3

trend, but EEMD method revealed its changing trend from decreasing to increasing. Simple straight line fitting may have magnified the LAI decreasing speed and amplitude.

Regional-averaged forest LAI variations

Regional-averaged forest LAI were decomposed using EEMD and compared in terms of the increment value and instantaneous rate of trend, which could reflect regional difference of LAI variations related to the eco-geographical conditions and climate changes. From Fig. 6a, except that tropical humid region and temperate humid/subhumid region started the trends with slightly accumulated decrease, all other regions presented accumulative increasing LAI. During the early years, forest LAI increased fastest in the north subtropical humid region and Tibetan Plateau region, where the increment was always significant. The increment of LAI trend in north subtropical humid region first of all exceeded 0.15, and that in Tibetan Plateau region was maintained below 0.15. Temperate zone experienced short-time accumulated decrease before 1987 and changed smoothly with low increment values for a relatively long time, until increasing significantly for the last 2 years. Tropical zone transferred from accumulated decrease to increase in 1990 and then increased quickly. At the end of the study period, LAI in the south subtropical humid region increased dramatically with increment first reaching above 0.3 in 2007.

Corresponding to Fig. 6a, Fig. 6b shows that the instantaneous rate in tropical humid region first decreased and then increased, while temperate humid/subhumid region experienced a more complicated trend process with at least three turning points, and other regions basically reflected different variations dominated by rising trend with increasing rates. Forest LAI in the north subtropical humid region had positive rates all the time and reached to the lowest in the late 1990s. LAI increased most rapidly with the largest magnitude in the

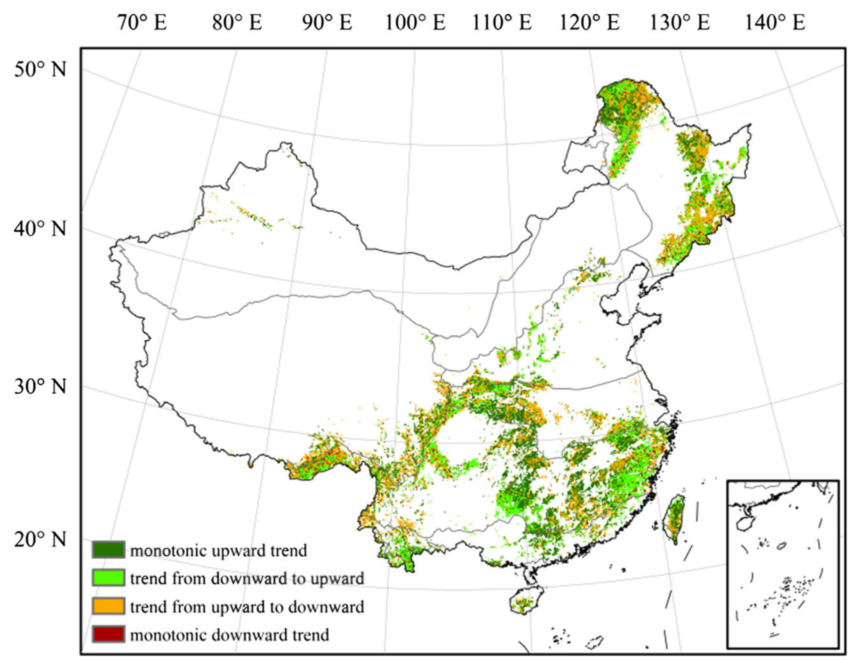

Fig. 5 EEMD trend types of forest LAI during 1982–2010

south subtropical and tropical humid regions when entering the twenty-first century. Only in the northwest arid region and Tibetan Plateau region LAI did rates shifted from positive to negative, indicating that forest LAI trend in the two regions was prone to decrease in the changing rate, despite keeping an increase of the increment value. Judging by the variations of EEMD residual trend, national-averaged forest LAI in China exhibited a continuously and steadily rising trend from 1982 to 2010 with an increasing rate, especially noticeable in the accumulated increase during the last 10 years.

Discussion

EEMD, one of the advanced time-frequency analysis methods in the field of climate change, has been introduced into vegetation dynamic research in this study, focusing on the nonlinear trend variations of forest LAI in China. On the one hand, through decomposing on pixel scale and specifying typical times, the spatial-temporal evolution of LAI trend variations was displayed. On the other hand, based on eco-geographical regions and pixel area-weighted averaging, the accumulated

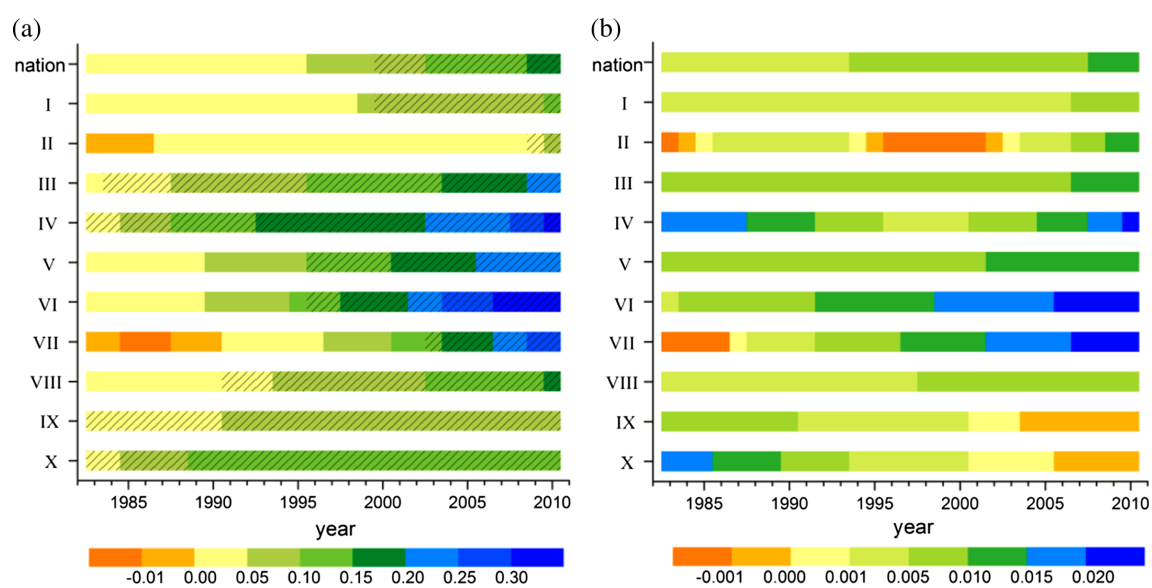

Fig. 6 Forest LAI increment (**a**) and changing rate (**b**) of eco-geographical regions based on EEMD trend. Note that shadows represent significant increment values

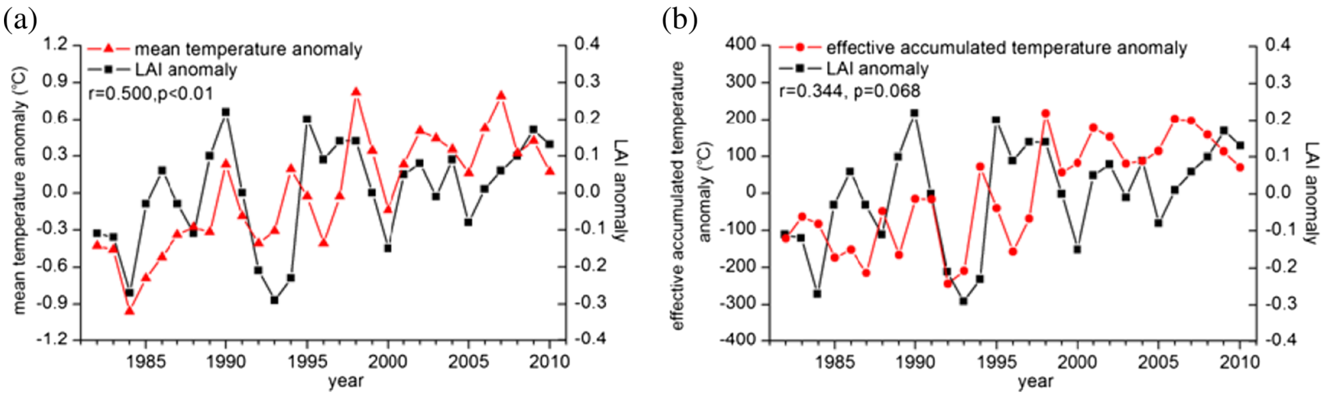

Fig. 7 Comparisons between mean temperature anomaly (**a**), effective accumulated temperature anomaly (**b**), and forest LAI anomaly over China. Note that *r* denotes the Pearson correlation coefficient

change and trend speed were clarified. Forest vegetation growth reflected in this study was consistent with the increasing trend of forest carbon storage in China estimated by forest inventory and model simulations (Li et al. 2009; Xu et al. 2007; Zhao et al. 2013). This was predominantly explained by the increasing warming rate over China in the past decades (Li et al. 2010; Wang et al. 2010), and because of that, the increase of effective accumulated temperature in duration and sum total may accelerate forest vegetation activities in China (Liu et al. 2013). The interannual oscillations of forest LAI, which were close to the 2~7-year cycle of ENSO, may suggest responses of vegetation activity to ENSO events. Studies showed that ENSO phase transition was the prime driver of regional climate change and influenced vegetation growth through directly altering localized temperature and precipitation (Nagai et al. 2007; Pompa-García et al. 2015). The original series and high-frequency IMF components fluctuated wildly with largest amplitudes in the early 1990s, which may be related to the Pinatubo volcano eruption in 1991. Studies found that the temporary cooling effect caused by volcano eruption may result in abrupt decrease of LAI and NPP (Guenet et al. 2013; Lucht et al. 2002).

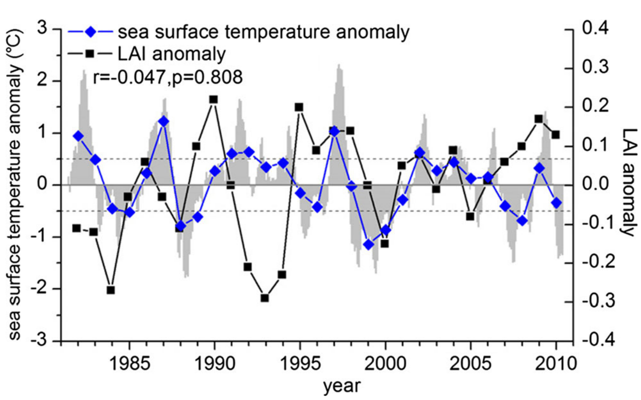

Fig. 8 Comparison between sea surface temperature anomaly over Nino 3.4 region and forest LAI anomaly over China. ENSO events occur when monthly sea surface temperature anomalies (*gray bars*) are larger than 0.5 °C in magnitude for several months. Note that *r* denotes the Pearson correlation coefficient

Here, we checked the correlations between forest LAI and temperature variables for the study area as a whole and found LAI was significantly positively related to annual mean temperature (Fig. 7a). Figure 7b also shows a relationship ($r = 0.344$, $p = 0.068$) between LAI and annual effective accumulated temperature (≥10 °C), which was calculated based on the homogenized daily temperature data of meteorological stations in China. Using sea surface temperature anomaly over Nino 3.4 region downloaded from NOAA's Climate Prediction Center to represent ENSO activity, we compared it with national-averaged forest LAI anomalies, but there was no statistically significant correlation between them (Fig. 8). This may be partly due to that ENSO events usually occuring in an irregular interannual cycle and having a lagging impact on vegetation changes. Since the periodic components of climate factors decomposed by EEMD might not correspond exactly to those of forest LAI, it can be hard to investigate the impact of climate change in different characteristic scales on vegetation, with such a relatively short time span. NDVI-based analyses suggested that the sensitivity of vegetation to ENSO varied across ecosystems in China and differed between El Niño and La Niña events, but other environmental changes at local and regional scales may yet obscure the impacts of ENSO activities on vegetation (Lü et al. 2012; Meng et al. 2011). We will further examine their potential relationship in other ways and improve the explanation in the next studies.

In addition to climate change, atmospheric composition change may also have impacts on vegetation dynamics. Rising CO_2 concentration and nitrogen deposition are considered to have accelerated photosynthesis and greening in China for the past decades, particularly in the southern area (Jia et al. 2014; Piao et al. 2015). However, it should be noted that in the current study, the interactions between different drivers of vegetation change have not been fully taken into account when measuring their contributions. Moreover, land conversions, farming and grazing, and environment protections may cause improvement or degradation of vegetation.

Deforestation and afforestation will play an important role in forest management and ecological restoration (Lu et al. 2015; Mueller et al. 2014). For example, human activities exhibited two opposite effects on the vegetation dynamics of Xinjiang, which are vegetation regeneration in oases and desertification in alpine meadows (Guli et al. 2015); Socioeconomic polices and human activities were found to have contributed to greenness increase and vegetation growth over the Loess Plateau region in the 2000s (Fan et al. 2015). Objectively analyzing driving mechanism of forest vegetation change needs to take human impact into account. Nevertheless, it is difficult to directly distinguish human-induced change from climate effects, considering the complex feedbacks between them. Further analysis and discussion about quantitative assessment for the effects of climate and humans on forest LAI change is required.

The LAI3g dataset used in this study was mainly based on the NDVI3g dataset, which has experienced calibrations and corrections for orbital drift artifacts, volcanic aerosol effects, cloud contamination, and other issues (Zeng et al. 2013). Through the combination of AVRHH NDVI and MODIS LAI for an overlapping period, the long-term consistent LAI3g product was produced by means of a neural network algorithm. Its utility has been documented by comparing with simulations from various ecological models in different latitudes (Anav et al. 2013; Mao et al. 2013). However, the inconsistency among different sensors may raise uncertainty during the process of multisource data fusion, due to the differences in spectral response, data quality, and band information (Liu et al. 2012b). Besides, the satellite orbit loss was proved to have an influence on investigating the interannual variability of LAI3g and its relationship with climatic variables. When used in generating LAI3g, the constant land cover map lacked consideration for the land cover change during the past three decades. These may also lead to some uncertainties of our study.

Conclusions

This study used EEMD method to analyze temporal-spatial variations of forest LAI in China and explored its regional differences from the perspective of eco-geographical regions. The main conclusions are summarized as follows:

1. In the past 29 years, national-averaged forest LAI in China had quasi-3- and quasi-7-year oscillations, which overall exhibited a rising trend with an increasing rate.
2. The increment value and instantaneous rate of LAI trend showed obvious regional difference and time-varying feature. Areas with significant accumulated change in 1982–2010 exceeded those in 1982–1990 and 1982–2000, where Central and South China reached the maximum increments. The extent and range of LAI changing rates in 2010 were greater than those in 1990 and 2000, and the fastest increasing speed occurred in the southeastern coastal areas. EEMD trend shapes of forest LAI were classified into four types. For most areas in China, forest LAI first decreased and then increased or vice versa, and for a small number of regions, forest LAI increased or decreased monotonically.
3. With regard to the increment value and instantaneous rate of LAI trend among eco-geographical regions, except that LAI had transferred from accumulative decrease to increase in tropical humid region and temperate humid/subhumid region, all other regions showed increasing trends in LAI with different magnitudes and speeds from the start of the study period. In the first half of the period, forest LAI increased fastest in the north subtropical humid region and Tibetan Plateau region. While in the second half, forest LAI in the south subtropical humid region and tropical humid region achieved the rapidest pace. By the year 2010, all regions exhibited a significant rising trend in LAI relative to 1982.
4. Through comparison with annual mean temperature and annual effective accumulated temperature, forest LAI in China was positively affected by the warming climate during 1982–2010. The impact of ENSO events on the forest LAI in China was not that obvious.

Acknowledgements This work was supported by the National Natural Science Foundation of China (41571043), the Key Program of National Natural Science Foundation of China (41530749), and the National Science and Technology Support Program (grants 2012BAC19B02).

References

Anav A, Murray-Tortarolo G, Friedlingstein P et al (2013) Evaluation of land surface models in reproducing satellite derived leaf area index over the high-latitude Northern Hemisphere. Part II: Earth system models. Remote Sens 5:3637–3661

Barr AG, Black TA, Hogg EH et al (2004) Inter-annual variability in the leaf area index of a boreal aspen-hazelnut forest in relation to net ecosystem production. Agric For Meteorol 126:237–255

Bonan GB (2008) Forests and climate change: forcings, feedbacks, and the climate benefits of forests. Science 320:1444–1449

Bradley BA, Jacob RW, Hermance JF et al (2007) A curve fitting procedure to derive inter-annual phenologies from time series of noisy satellite NDVI data. Remote Sens Environ 106:137–145

Buermann W, Dong J, Zeng X et al (2001) Evaluation of the utility of satellite-based vegetation leaf area index data for climate simulations. J Clim 14:3536–3550

Campioli M, Michelsen A, Samson R et al (2009) Seasonal variability of leaf area index and foliar nitrogen in contrasting dry-Mesic tundras. Botany 87:431–442

Chang CY, Chiang JCH, Wehner MF et al (2010) Sulfate aerosol control of tropical Atlantic climate over the twentieth century. J Clim 24: 2540–2555

Chen JM, Cihlar J (1996) Retrieving leaf area index of boreal conifer forests using Landsat TM images. Remote Sens Environ 55:153–162

Fan X, Ma Z, Yang Q et al (2015) Land use/land cover changes and regional climate over the Loess Plateau during 2001–2009. Part I: observational evidence. Clim Chang 129:441–455

Fang H, Wei S, Jiang C (2012) Intercomparison and uncertainty analysis of global MODIS, cyclopes, and GLOBCARBON LAI products. 2012 I.E. International Geoscience and Remote Sensing Symposium (IGARSS), Munich, Germany, July 22–27, pp. 5959–5962

Franzke C (2012) Nonlinear trends, long-range dependence, and climate noise properties of surface temperature. J Clim 25:4172–4183

Friedl MA, Sulla-Menashe D, Tan B et al (2010) MODIS collection 5 global land cover: algorithm refinements and characterization of new datasets. Remote Sens Environ 114:168–182

Guenet B, Cadule P, Zaehle S et al (2013) Does the integration of the dynamic nitrogen cycle in a terrestrial biosphere model improve the long-term trend of the leaf area index? Clim Dynam 40:2535–2548

Guli J, Liang S, Yi Q et al (2015) Vegetation dynamics and responses to recent climate change in Xinjiang using leaf area index as an indicator. Ecol Indic 58:64–76

Hawinkel P, Swinnen E, Lhermitte S et al (2015) A time series processing tool to extract climate-driven interannual vegetation dynamics using ensemble empirical mode decomposition (EEMD). Remote Sens Environ 169:375–389

Henebry GM, Beurs KMD (2005) A statistical framework for the analysis of long image time series. Int J Remote Sens 26:1551–1573

Huang M, Ji J (2010) The spatial-temporal distribution of leaf area index in China: a comparison between ecosystem modeling and remote sensing reversion. Acta Ecol Sin 30:3057–3064

IPCC (2007) Climate change 2007: impacts, adaptation and vulnerability. Contribution of working group II to the fourth assessment report of the intergovernmental panel on climate change. Cambridge University Press, Cambridge

Jamali S, Jonsson P, Eklundh L et al (2015) Detecting changes in vegetation trends using time series segmentation. Remote Sens Environ 156:182–195

Jamali S, Seaquist J, Eldundh L et al (2014) Automated mapping of vegetation trends with polynomials using NDVI imagery over the Sahel. Remote Sens Environ 141:79–89

Ji F, Wu Z, Huang J et al (2014) Evolution of land surface air temperature trend. Nat Clim Chang 4:462–466

Jia Y, Yu G, He N et al (2014) Spatial and decadal variations in inorganic nitrogen wet deposition in China induced by human activity. Sci Rep 4:3763–3763

Jong RD, Verbesselt J, Schaepman ME et al (2012) Trend changes in global greening and browning: contribution of short-term trends to longer-term change. Glob Change Biol 18:642–655

Lü A, Zhu W, Jia S (2012) Assessment of the sensitivity of vegetation to el-Niño/Southern oscillation events over China. Adv Space Res 50:1362–1373

Lasaponara R (2006) On the use of principal component analysis (PCA) for evaluating interannual vegetation anomalies from SPOT/VEGETATION NDVI temporal series. Ecol Model 194:429–434

Li Q, Dong W, Li W et al (2010) Assessment of the uncertainties in temperature change in China during the last century. Chinese Sci Bull 55:1974–1982

Li X, Zhou T, He X (2009) Carbon sink of forest ecosystem driven by NPP increasing in China. Journal of Natural Resources 24:491–497

Liu S, Liu R, Yang L (2010) Spatial and temporal variation of global LAI during 1981–2006. J Geogr Sci 20:323–332

Liu SH, Yan DH, Weng BS et al (2013) Spatiotemporal evolution of effective accumulated temperature ≥ 10 °C in China in recent 50 years. Arid Zone Research 30:689–696

Liu Y, Ju W, Chen J et al (2012a) Spatial and temporal variations of forest LAI in China during 2000–2010. Chinese Sci Bull 57:1435–1445

Liu Y, Liu R, Chen JM (2012b) Retrospective retrieval of long-term consistent global leaf area index (1981–2011) from combined AVHRR and MODIS data. Journal of Geophysical Research Biogeosciences 117(G04003):1–14

Lu Y, Zhang L, Feng X et al (2015) Recent ecological transitions in China: greening, browning, and influential factors. Sci Rep 5:1–8

Lucht W, Prentice IC, Myneni RB et al (2002) Climatic control of the high-latitude vegetation greening trend and Pinatubo effect. Science 296:1687–1689

Mao J, Shi X, Thornton PE et al (2013) Global latitudinal-asymmetric vegetation growth trends and their driving mechanisms: 1982–2009. Remote Sens 5:1484–1497

Martínez B, Gilabert MA (2009) Vegetation dynamics from NDVI time series analysis using the wavelet transform. Remote Sens Environ 113:1823–1842

Meng M, Ni J, Zong M (2011) Impacts of changes in climate variability on regional vegetation in China: NDVI-based analysis from 1982 to 2000. Ecol Res 26:421–428

Millar CI, Stephenson NL, Stephens SL (2007) Climate change and forests of the future: managing in the face of uncertainty. Ecol Appl 17:2145–2151

Monteith JL, Unsworth MH (1990) Principles of environmental physics. Edward Arnold, London

Mueller T, Dressler G, Tucker CJ et al (2014) Human land-use practices lead to global long-term increases in photosynthetic capacity. Remote Sens 6:5717–5731

Muraoka H, Saigusa N, Nasahara KN et al (2010) Effects of seasonal and interannual variations in leaf photosynthesis and canopy leaf area index on gross primary production of a cool-temperate deciduous broadleaf forest in Takayama, Japan. J Plant Res 123:563–576

Murray-Tortarolo G, Anav A, Friedlingstein P et al (2013) Evaluation of land surface models in reproducing satellite-derived LAI over the high-latitude Northern Hemisphere. Part I: uncoupled DGVMs. Remote Sens 5:4819–4838

Nagai S, Ichii K, Morimoto H (2007) Interannual variations in vegetation activities and climate variability caused by ENSO in tropical rainforests. Int J Remote Sens 28:1285–1297

Piao S, Friedlingstein P, Ciais P et al (2006) Effect of climate and CO2 changes on the greening of the northern hemisphere over the past two decades. Geophys Res Lett 33:265–288

Piao S, Yin G, Tan J et al (2015) Detection and attribution of vegetation greening trend in China over the last 30 years. Glob Change Biol 21:1601–1609

Pompa-García M, Miranda-Aragón L, Aguirre-Salado C (2015) Tree growth response to ENSO in Durango, Mexico. Int J Biometeorol 59:89–97

Qian C, Fu C, Wu Z et al (2011) The role of changes in the annual cycle in earlier onset of climatic spring in Northern China. Adv Atmos Sci 28:284–296

Ren H, Shi X, Zhang Z (2014) Analysis of leaf area index variations over China during 2003-2009. Journal of the Meteorological Sciences 34:171–178

Sellers PJ, Randall DA, Betts AK et al (1997) Modeling the exchanges of energy, water, and carbon between continents and the atmosphere. Science 275:502–509

Shi F, Li J, Wilson RJS (2014) A tree-ring reconstruction of the South Asian summer monsoon index over the past millennium. Sci Rep 4:1–8

Shi F, Yang B, Lv G et al (2012) Ensemble empirical mode decomposition for tree-ring climate reconstructions. Theor Appl Climatol 109:233–243

Verbesselt J, Hyndman R, Newnham G et al (2010) Detecting trend and seasonal changes in satellite image time series. Remote Sens Environ 114:106–115

Verma R, Dutta S (2013) Vegetation dynamics from denoised NDVI using empirical mode decomposition. J Indian Soc Remote Sens 41:555–566
Wang SP, Wang ZH, Piao SL et al (2010) Regional differences in the timing of recent air warming during the past four decades in China. Chinese Sci Bull 55:1968–1973
Wu Z (1980) Vegetation of China. Science Press, Beijing
Wu Z, Huang NE (2004) A study of the characteristics of white noise using the empirical mode decomposition method. P Roy Soc Lond A 460:1597–1611
Wu Z, Huang NE (2009) Ensemble empirical mode decomposition: a noise-assisted data analysis method. Advances in Adaptive Data Analysis 01:1–41
Wu Z, Huang NE, Wallace J et al (2011) On the time-varying trend in global-mean surface temperature. Clim Dynam 37:759–773
Xia J, Yan Z, Wu P (2013) Multidecadal variability in local growing season during 1901–2009. Clim Dynam 41:295–305
Xiao J, Moody A (2010) Trends in vegetation activity and their climatic correlates: China 1982 to 1998. Int J Remote Sens 25:5669–5689
Xu X, Cao M, Li K (2007) Temporal-spatial dynamics of carbon storage of forest vegetation in China. Prog Geogr 26:1–10
Zeng FW, Collatz GJ, Pinzon JE et al (2013) Evaluating and quantifying the climate-driven interannual variability in global inventory modeling and mapping studies (GIMMS) normalized difference vegetation index (NDVI3g) at global scales. Remote Sens 5:3918–3950
Zhao M, Yue T, Zhao N et al (2013) Spatial distribution of forest vegetation carbon stock in China based on HASM. Acta Geograph Sin 68: 1212–1224
Zheng D (2008) China's Ecogeographical regionalization research (in Chinese). The Commercial Press, Beijing
Zhu Z, Bi J, Pan Y et al (2013) Global data sets of vegetation leaf area index (LAI)3g and fraction of photosynthetically active radiation (FPAR)3g derived from global inventory modeling and mapping studies (GIMMS) normalized difference vegetation index (NDVI3g) for the period 1981 to 2011. Remote Sens 5:927–948